

Dynamical Properties of a Buoyancy-Driven Coastal Current

ANDREAS MÜNCHOW AND RICHARD W. GARVINE

University of Delaware, College of Marine Studies, Newark

The outflow of buoyant waters from major estuaries affects the dynamics of inner continental shelves profoundly as lateral density gradients force an alongshore current. Often the Coriolis force causes the outflow to remain trapped near the coast. We observed one such current, the Delaware Coastal Current, on the inner shelf near the Delaware Estuary on the eastern seaboard of the United States. The spatial variability along the shelf, however, suggests at least two dynamically distinct regions that we term source and plume regions. In the source region we find fronts, a current whose width scales well with the internal deformation radius, and a ratio of relative to planetary vorticity that reaches unity, that is, the Rossby number is $O(1)$. As nonlinear inertial forces in the across-shelf momentum balance are weak, we suggest that such forces contribute to the along-shelf momentum balance only. Farther downstream in the plume region, we find much reduced lateral density gradients, a current much wider than the deformation radius, and relative vorticities that are much smaller than the planetary vorticity. From our observations we compute nondimensional dynamical parameters, with which we discuss our observations. The Burger, Rossby, and Ekman numbers for the Delaware Coastal Current suggest that most models of buoyancy-driven coastal currents do not apply to this coastal flow.

I. INTRODUCTION

The lateral flux of buoyancy from estuaries into the coastal ocean constitutes a forcing agent influencing both circulation and mixing. The density differences between brackish estuarine and salty oceanic waters force a flow on the shelf. Density gradients induce pressure gradients which are often balanced by Coriolis forces. In the northern hemisphere the Coriolis force turns the estuarine outflow to the right looking seaward and traps the buoyant water on the inner shelves. Across-shelf mixing with ambient shelf water is thus reduced. Such currents distribute riverborne nutrients, larvae, sediments, sewage, toxic chemicals, and oil from accidental spills dominantly along the shore. This study will describe one such current, namely the Delaware Coastal Current.

Woods and Beardsley [1988] studied barotropic estuarine outflow problems with a set of analytical, numerical, and laboratory experiments. The outflowing fluid enters a uniformly sloping shelf, where vortex tube stretching and friction determine its path. Their studies relate indirectly to the discharge of water from major rivers, since they isolate barotropic from baroclinic effects. For small Rossby numbers, they found that *Csanady's* [1978] arrested topographic wave dynamics resulted, whereas for moderate Rossby numbers they reproduced the one-layer results of *Beardsley and Hart* [1978]. *Beardsley and Hart* prescribed an outflow from a point source, while *Woods and Beardsley* [1988] modeled the shelf flow that was forced by an outflow from a finite gap in the coastline. In both studies estuarine waters turn to the right in the northern hemisphere.

Most outflows, however, are not barotropic but transport buoyancy into the coastal ocean. Observations of buoyant outflows consistently stress the close correlation of coastal

currents with buoyancy sources upstream. *Simpson and Hill* [1986] sketched the outflow of buoyant Irish Sea water along the west coast of Scotland to the north. There, a buoyancy driven, weak, but stable current system branches when it encounters a gap in the coastline. Also in Europe, the Rhine outflow forms a coastal current that influences the entire Dutch coastal zone [*Simpson et al.*, 1993; *van der Giessen et al.*, 1990]. For the South Atlantic Bight on the eastern seaboard of the United States *Blanton* [1981] describes observations of a buoyancy-driven coastal current in thermal wind balance. *Doyle and Wilson* [1978] analyze data from a transect across the mouth of the Hudson River. This outflow forms a coastal current which *Bowman and Iverson* [1978] trace on the shelf. *Masse and Murthy* [1990] describe the buoyant outflow of the Niagara River into Lake Ontario. The temperature difference between the two bodies of water induces baroclinic pressure gradients that are balanced by an alongshore current. These flows all appear similar to the Delaware Coastal Current because the buoyant layer depths are all of the same order as the water depth.

In contrast, most buoyant flows occupy only a small portion of the water column: *Hickey et al.* [1991] attributed about 15% of the variance of the Vancouver Island Coastal Current to buoyancy forcing from the Fraser River, British Columbia. *Johannessen et al.* [1989] and *Mork* [1981] described the Norwegian Coastal Current, and *Royer* [1983], *Johnson et al.* [1988], and *Ahlén et al.* [1987] studied the Alaska Coastal Current, its seasonal variability, and its instability, respectively. *Tang* [1980] and *Mertz et al.* [1988] studied the hydrography, evolution, and instabilities of the Gaspé Current in Canada. This current derives its buoyancy from the St. Lawrence River and appears as a shallow, buoyancy-driven coastal jet which emerges from the classical vertical two-layer gravitational circulation [*Hansen and Rattray*, 1965] under the influence of the Coriolis force.

At the offshore edge of buoyant outflows the depth of the upper layer or plume often vanishes abruptly and forms a front with oceanic waters offshore. *Garvine* [1987] investi-

Copyright 1993 by the American Geophysical Union.

Paper number 93JC02112.
0148-0227/93/93JC-02112\$05.00

gated the dynamics of such plumes with a reduced-gravity, steady state, layer model. He treated fronts as discontinuities where frictional dissipation takes place. O'Donnell [1988] developed a numerical layer model which simulates time-dependent plume dynamics and fronts. There is a fundamental physical difference between reduced gravity [Garvine, 1987; O'Donnell, 1988] and barotropic [Woods and Beardsley, 1988] models. For the former, bottom friction is usually negligible so that potential vorticity is conserved. Thus, an offshore traveling water parcel gains anticyclonic vorticity owing to vortex tube squashing, since the upper layer depth decreases offshore toward the density front. In contrast, for the barotropic case, bottom friction is a major term in the vorticity balance and, further, an offshore parcel gains cyclonic vorticity owing to vortex tube stretching because the total water depth increases offshore. Bottom friction diffuses relative vorticity and thus widens the outflow on the shelf [Woods and Beardsley, 1988]. Finally, for a baroclinic current that extends to the bottom, no simple interpretation is possible as now both a barotropic and a baroclinic response may occur. In the absence of upwelling favorable winds the Delaware Coastal Current is of the latter form. It widens from one to several internal deformation radii, from what we term a source to a plume region. We will interpret the increasing width of the buoyant flow as a result of bottom friction since the current contacts the bottom in the absence of upwelling favorable winds. This makes our buoyant flow different from many others. The buoyant surface layer of the Alaska Current, the Norwegian Current, the Vancouver Island Current, the Gaspé Coastal Current, as well as the Chesapeake outflow, is well isolated from the bottom Ekman layer since their "plume" depth is much smaller than the total water depth. In contrast, in the Delaware Coastal Current the buoyant layer depth compares with both the total water and the Ekman layer depths.

The wealth of theoretical [Weaver and Hsieh, 1987; Chao, 1988b; Galperin and Mellor, 1990a,b] and laboratory [Griffiths and Linden, 1981; Whitehead and Chapman, 1986] studies on buoyancy-driven coastal currents would appear to treat all possibilities. However, as we discuss in section 5, most of these and other studies do not apply to coastal currents of moderate strength on shallow continental shelves where Ekman numbers are $O(1)$. Such flows, however, are common: The Delaware [Garvine, 1991] and Hudson [Doyle and Wilson, 1978] River outflows, the South Atlantic Bight coastal current [Blanton, 1981], the Scottish Coastal Current [Simpson et al., 1989], and the Rhine outflow [Simpson et al., 1993] all belong to this group; they have not yet been modeled satisfactorily, because their detailed dynamics is unknown.

This paper will describe the formation of the Delaware Coastal Current, a buoyancy-driven coastal current in water that is less than 30 m deep. We observed this current in 1989 with shipboard and moored instruments and by tracking surface drifters. In subsequent sections we first present selected aspects of the flow in order to make a clear observational statement rather than describing all the observed variability. Instead, we compute nondimensional parameters that characterize all the data. We will define Rossby, Burger, and Froude numbers, present their variability along the coast, and distinguish two dynamically different regimes that the parameters imply. In section 2 we define these parameters and introduce the study area and data sources. In

sections 3 and 4 we discuss the source and the plume regions, respectively. Section 5 concludes this study, speculates on a third region, and compares the observational results with models.

2. DATA SOURCES AND PARAMETERS

From March through June 1989 we studied the flow and density field in an area of expected strong buoyancy-driven flows in shallow water. The study area (Figure 1) centers on the mouth of the Delaware Estuary and extends 35 km offshore and 100 km alongshore. We collected both Eulerian and Lagrangian current data as well as more than 1000 hydrographic casts. The hydrographic sampling employed standard vertical conductivity-temperature-depth (CTD) profiling along transects as well as an underway thermosalinograph. Figure 1 shows the location of the major transects. The thermosalinograph measured temperature and salinity from water pumped at a depth of about 0.5 m.

A 307-kHz-ship mounted acoustic Doppler current profiler (ADCP) (RDI Inc., San Diego) and 10 moored InterOcean S4 current meters provided Eulerian current measurements. Münchow et al. [1992 b] describe the ADCP, its calibration, use, and performance, as well as the methodology to remove tidal currents from the data it returns. Figure 1 also shows the locations of six current meter moorings, four of which had two S4 meters attached to them at 6 and 10 m below the surface. The farthest offshore moorings on transects A and C had only a single instrument at a depth of 6 m. The moorings returned velocity, conductivity, and temperature data every half hour representing temporal averages of 5 min. While the S4 data lack spatial coverage, especially in the vertical direction, they have excellent temporal coverage. The reverse is true for the ADCP data. Hence these data sets complement each other.

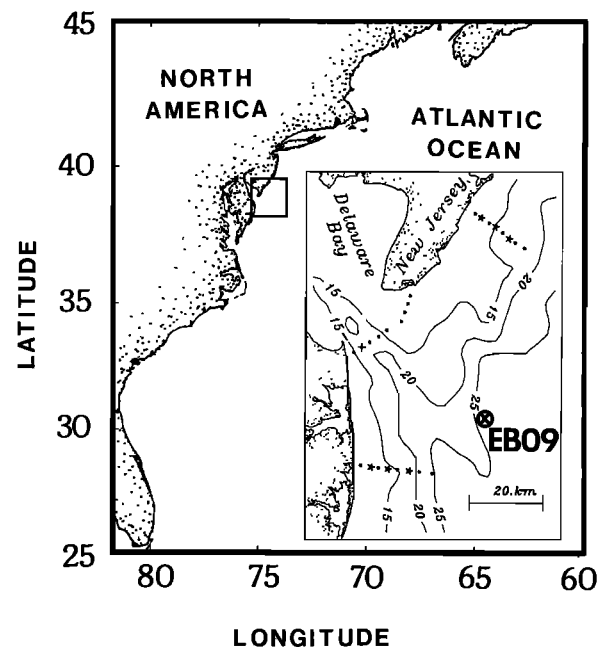


Fig. 1. Map of the study area. The insert is an enlargement of the area near 38°N and 75°W. We denote the three major transects as a, b, and c and current meter locations as solid stars on transects A and C. The dots on each transect mark the location of an ADCP and CTD station. EB9 represents a meteorological buoy.

Because we formulate all observational results in terms of independent nondimensional parameters, we define them here as ratios of different length scales. Each of these scales measure the influence of a physical process that contributes to the often complex flow and density field of the coastal current. We will next define Rossby, Burger, and vertical Ekman numbers, which originate from scaling analysis of the governing momentum and vorticity equations [Pedlosky, 1987]. Laboratory [d'Hieres *et al.*, 1991] and theoretical [Hogg, 1973; Chao, 1988a] studies often use these numbers. We believe that observational studies such as this one are concisely summarized by these three parameters.

The internal deformation radius we define as

$$L_D \equiv ND/f \quad (1)$$

where N is the stability, buoyancy, or Brunt-Väisälä frequency, that is,

$$N^2 \equiv -(g/\rho_0) \partial_z \rho \quad (2)$$

and D , f , and ρ are water depth, Coriolis parameter, and density, respectively. The reference density ρ_0 is 1025.5 kg/m³. Our definition of L_D follows that of Pedlosky [1987] where D is the vertical scale of motion. In our application this scale is the depth of the entire water column. A second length scale is the inertial radius L_i , which depends upon a velocity scale U :

$$L_i \equiv U/f. \quad (3)$$

This scale represents nonlinear inertial forces. A third independent length scale of the coastal current is the distance L of buoyant waters from the coast. In an inviscid, linear, and steady system $L \rightarrow L_D$ [Gill, 1976]. Generally, however, the two scales may differ, as indeed they do in the present application. We speculate that frictional stresses widen the buoyant waters on the shelf. This process represents the diffusion of relative vorticity. All three length scales range between 2 and 30 km and are thus much smaller than the shelf width, which is more than 100 km in the Mid-Atlantic Bight. This latter geometric scale is thus unimportant for the dynamics of the coastal current.

From the three horizontal length scales L_D , L_i , and L we define two nondimensional parameters, namely a Burger number and a Rossby number. The Burger number

$$S = (L_D/L)^2 \quad (4)$$

measures the influence of stratification on the vorticity dynamics [Pedlosky, 1987]. The Rossby number

$$\epsilon \equiv L_i/L \quad (5)$$

measures the strength of nonlinear inertial relative to Coriolis accelerations. The use of a bulk scale for velocity U , however, underestimates the strength of inertial forces in horizontally sheared flows. Hence we use a second, independently determined estimate of the Rossby number that accounts for horizontal shear. From transect data we first compute transverse current shears. These we then interpret as estimates of the relative vorticity ξ . The ratio ξ/f

then constitutes an alternative measure of inertial to Coriolis forces, that is, a Rossby number. The internal Froude number

$$F = U/C \quad (6)$$

measures the ratio of particle and internal wave speeds. Here $C = ND$ is the phase speed of an internal perturbation. For a strongly nonlinear, baroclinic flow, particle speeds exceed internal phase speeds and the flow is termed "supercritical". In our formulation, however, this parameter depends upon ϵ and S , that is,

$$F = \epsilon S^{-1/2} = L_i/L_D. \quad (7)$$

From our three horizontal length scales we have thus defined two independent dynamical parameters that describe the respective importance of baroclinicity, nonlinear inertial forces, and Coriolis forces.

In a turbulent flow the Ekman layer depth δ and the water depth D define still another nondimensional parameter, namely, the vertical Ekman number E , where

$$E \equiv (\delta/D)^2 \quad (8)$$

$$\delta \equiv (2A/f)^{1/2} \quad (9)$$

and A is a vertical eddy viscosity. We have then defined three independent parameters, S , ϵ , and E which describe buoyancy driven coastal currents. The alongshore variability of the former two parameters distinguishes successive stages of the formation process. In the source region the flow is moderately stratified and nonlinear, that is, $S = O(1)$ and ϵ can be large, whereas downstream in the plume region the flow appears weakly stratified and linear: S and ϵ are both small relative to 1. We next discuss the source region.

3. THE SOURCE REGION

3.1. Observations

On short timescales, strong fronts are an important feature of the source region near the estuary mouth. Figure 2 documents such a front that separates different water masses. The ship track shown in Figure 2 began in ambient shelf waters that were both warm (18.5°C) and salty (31 practical salinity units (psu)) near the surface. Thereafter water temperatures decreased slowly to 15°C while salinities stayed constant as the ship passed a tidal mixing zone near the shoals off New Jersey, discussed in much detail by Münchow *et al.* [1992a]. Finally, after crossing the front the ship entered a third water mass, namely, the buoyant outflow from the estuary. Both temperature and salinity changed dramatically. The 4-psu and 4° ± 1°C change in salinity and temperature, respectively, correspond to a density difference of about 4.5 ± 0.2 kg/m³ over scales that are 0(100 m). The density field is thus strongly frontal.

In contrast we show the subtidal density distribution for transect B in Figure 3 for three sampling periods in March, April, and June 1989. Each month we profiled the transect eight times within a day and fitted a subtidal mean and a tidal oscillation to the data at each point of the transect.

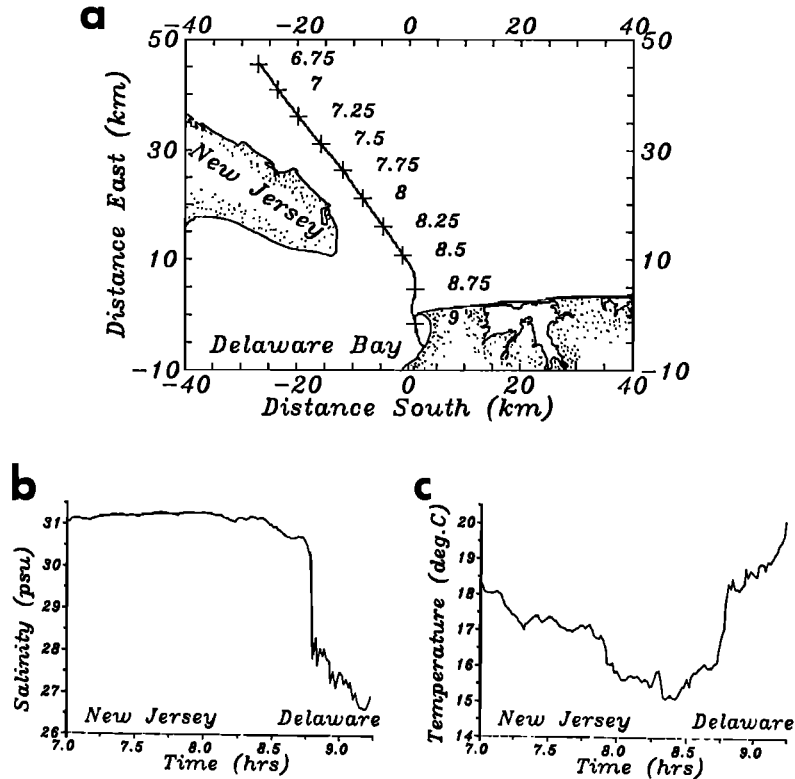


Fig. 2. The front of the source region on June 18, 1989: (a) Ship track, labels indicate local time of the day in hours; (b) Time series of salinity along the ship track; (c) Time series of temperature along the ship track. The change of salinity and temperature at 8.75 hours represents a decrease of density by more than 4 kg/m^3 .

Münchow *et al.* [1992b] discuss the method in detail. From the three subtidal density transects in Figure 3 a weak seasonal signal emerges as the vertical stratification on the shelf changes from winter to summer conditions. The particular values do not concern us here, but the general pattern does. We find lighter water concentrated on the Delaware side of the estuary near the deeper channel. Largest lateral density gradients occur 8 km from that shore where we found the front shown in Figure 2. Analysis of the relation between temperature and salinity (not shown) indicates that three water masses are shown in Figure 3, namely warm and fresh river waters, warm and salty surface shelf waters, and, fi-

nally, cold and salty bottom shelf waters. The light buoyant waters over the deep channel represent a mixture of river and bottom shelf waters whereas the waters over the shoals represent a mixture of bottom and surface shelf waters. The buoyant waters over the deep channel correspond to a seaward flowing jet with speeds about 15 to 20 cm/s. This jet is vertically fairly uniform over the central portion of the water column [Münchow *et al.*, 1992b]. Hence the vertically averaged current vectors shown in Figure 4 are little different from the flow at a depth of 5m. We observed the jet at the same location in April (Figure 4), in March, and in June (not shown). Coincident with the region of large

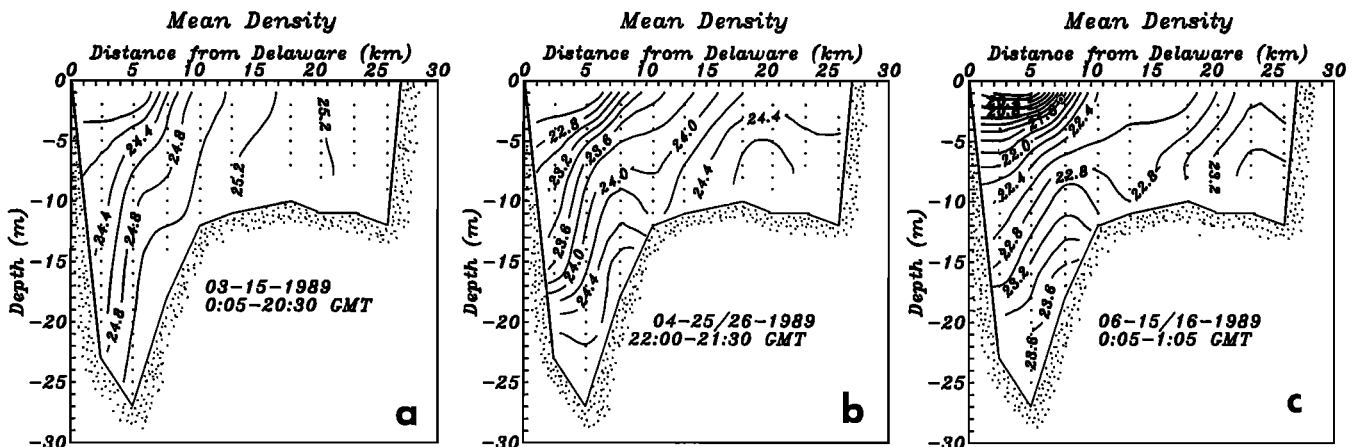


Fig. 3. Subtidal density σ_t for transect B across the mouth of the estuary in (a) March, (b) April, and (c) June of 1989. The view is landward with the Delaware coast on the left (see Figure 2). Contour interval is 0.2 kg/m^3 .

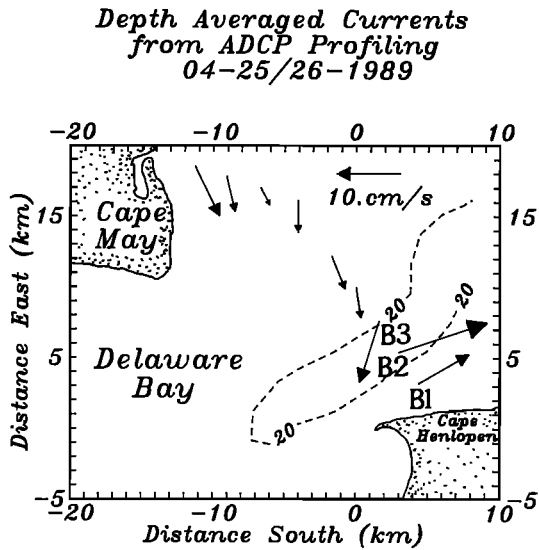


Fig. 4. Subtidal currents from ADCP profiling. Depth averaged current vectors are from April 1989 [from Münchow et al., 1992b]). Note the strong horizontal shear near the edge of the deep channel.

transverse density gradients is a region of large transverse current shear. A 10 cm/s landward flow at station B3 lies beside a 15 cm/s seaward flow at station B2 (Figure 4). These stations overlie two separate channels with a shallow ridge separating them. The ridge thus enhances strong lateral gradients that support the density driven circulation. The flow arrangement contrasts with results from theories that neglect the effect of rotation. Doyle and Wilson [1978] report similar results from the mouth of the Hudson River.

3.2. Dynamics

An inviscid, geostrophic flow in balance with its mass field would allow us to compute the alongshore velocity component relative to some level from a density transect alone. We test such a diagnostic thermal wind balance here for the source region by using detided velocity and density data from transect B. The geostrophic velocity gradient $\partial_x u_g$ due to the internal mass field is

$$\partial_x u_g = g \partial_y \rho / (\rho_0 f) \quad (10)$$

where u_g is the geostrophic velocity normal to transect B (positive seaward), y increases toward New Jersey, and z measures the vertical coordinate, positive up. We compare in Fig. 5 the observed shear with what we obtained from thermal wind balance dynamics. The ADCP measures only the central part of the water column away from boundaries, and our comparison is thus not complete. Nevertheless, the geostrophic shear varies between 0 and $2 \times 10^{-2} \text{ s}^{-1}$ whereas the shear from the ADCP scatters between -4×10^{-2} and $4 \times 10^{-2} \text{ s}^{-1}$. Most outliers, however, originate from locations where the water is less than 15 m deep. Later we discuss the observations that frictional forces become more important at these locations. Our test of geostrophy from thermal wind dynamics is thus not conclusive, and it is even possible that the flow is not geostrophic. To test this hypothesis, one needs better horizontal and vertical resolution of the current field.

To investigate the dynamics further, we next estimate the

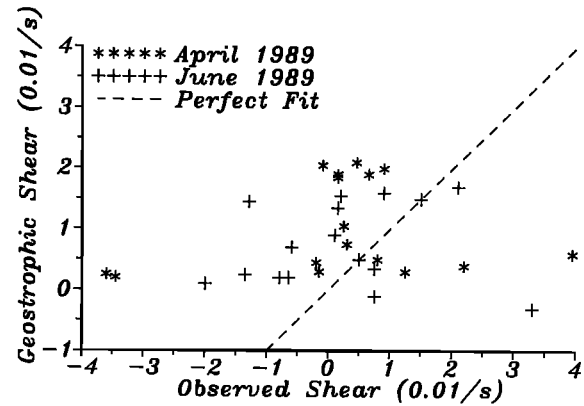


Fig. 5. Observed versus geostrophic vertical current shears. The observed current shears are from ADCP profiling; geostrophic shears originate from the thermal wind equation. The dashed line represents the perfect fit.

strength of other forces. The approach is not to seek closure of the dynamical balance but to obtain rough estimates of the magnitude of potentially important terms in the across-channel momentum balance. We exploit the observation that the subtidal flow is little sheared vertically [Münchow et al., 1992b] between 4 and 20 m below the surface in water 25 m deep. We thus diagnose depth-averaged dynamics of the source by assuming that the vertically averaged observed flow over part of the water column represents a depth-average well. We write the depth-averaged equation for the conservation of momentum across the channel as

$$\partial_t v + u \partial_x v + v \partial_y v + f u + g \partial_y \eta + g / (\rho_0 H) \int_{-H}^0 \int_{z'}^0 \partial_y \rho dz dz' \quad (11)$$

$$+ C_d v |v| / H + \langle U \partial_x V \rangle + \langle V \partial_y V \rangle + \langle V \partial_t \eta_T \rangle / H = 0$$

where (u, v) and (U, V) represent subtidal and tidal velocities, respectively, and η and η_T denote subtidal and tidal sea level perturbations. The angle brackets denote an average over a tidal cycle. The letters in parentheses identify the following terms: acceleration (a), nonlinear subtidal advection (b, c), Coriolis acceleration (d), barotropic (e) and baroclinic (f) pressure gradients, bottom friction (g), and tidal Reynolds stresses (h, i, j). The bottom friction coefficient C_d is taken as 2.5×10^{-3} . With the data on hand we cannot estimate terms a, b, e, or h. We estimated all other terms from ADCP data, normalized each term with the Coriolis term (d), and averaged each estimate over the transect. The results are depicted in Table 1. We estimated terms i and j by using predicted tidal currents that we obtained from the repeated ADCP profiling of the transect [Münchow et al., 1992b]. We estimate the error $\delta\psi$ of each term as

$$\delta\psi(\alpha_i) = \left| \frac{\partial\psi}{\partial\alpha_i} \right| \delta\alpha_i \quad (12)$$

where ψ is a term to be estimated. This term depends on measurements of N variables $\alpha_i \pm \delta\alpha_i$, $i = 1, 2, \dots, N$. This is clearly an upper bound of the error.

From Table 1 we infer that nonlinear inertial and frictional forces (terms c and g) are less than 10% of the Cori-

TABLE 1. Across-channel momentum balance.

	All B1 to B9	Channel B1, B2, B3	Shoals B3 to B9	Term
Term c	0.11 ± 0.09	0.04 ± 0.06	0.15 ± 0.12	$v\partial_y v$
Term f	0.53	2.65	0.29	$\int \int \partial_y \rho dz dz'$
Term g	0.12 ± 0.04	0.04 ± 0.02	0.20 ± 0.06	$C_d v v / H$
Term i	0.29 ± 2.91	0.18 ± 3.46	0.26 ± 2.85	$\langle V \partial_y V \rangle$
Term j	0.12 ± 0.08	0.80 ± 0.05	0.16 ± 0.11	$\langle V \partial_t \eta_T \rangle / H$

Absolute magnitude of terms in the across-channel momentum balance as estimated from CTD and ADCP data on transect B. All terms are scaled by the Coriolis acceleration, and terms c, f, g, i, and j are explained in the text.

olis acceleration. The two terms *i* and *j* representing tidal stresses [Nihoul and Ronday, 1974] are larger than inertial and frictional forces, but they, too, are small relative to the Coriolis term. The results, however, must be interpreted cautiously because the errors are large. The baroclinic pressure gradient approaches or exceeds the size of the Coriolis acceleration and thus is a major term in the across-shelf momentum balance at transect B. Doyle and Wilson [1978] estimate terms from a vertically differenced lateral momentum balance near the mouth of the Hudson River. They also discuss earlier literature on momentum balances in estuaries. In their study area, tidal stresses are small and the dynamics is dominated by baroclinic pressure gradients, Coriolis acceleration, and inertial accelerations. Their analysis, however, does not include the estimation of errors.

In the source region the buoyant waters represent a distinct water mass and a distinct flow regime. Therefore, we repeated the above analysis but interpreted the data in subregions, first from stations near the deep channel (B1 to B3) and second from those near the shoals (B3 to B9). We present the estimates for each subregion in Table 1 also. Over the shoals both bottom friction and nonlinear advection are sizable and tidal stresses contribute too. Nevertheless, no term alone rivals the Coriolis acceleration in the across-channel momentum balance there. We thus speculate that over the shoals many terms contribute to the across-channel momentum balance. In contrast, over the deep channel the balance is nearly geostrophic. Although both bottom friction and nonlinear advection are negligible, the baroclinic pressure gradient exceeds the Coriolis acceleration by a factor of 2.5. Hence a barotropic pressure gradi-

ent, which we cannot measure, is needed to oppose the large baroclinic pressure gradient. We thus speculate on a three term primary balance over the deep channel: sea surface slope, Coriolis acceleration, and baroclinic pressure gradient. The outflow along the channel would then be geostrophically balanced. Garrett and Petrie [1981] find a similar balance for the Strait of Belle Isle, Canada.

If nonlinear inertial forces were unimportant in both *x* and *y* directions, we would expect the flow to have a small Rossby number ϵ which, according to Pedlosky [1987, p. 345], is the ratio between the relative vorticity ξ and the planetary vorticity f : $\epsilon = \xi/f = (\partial_x v - \partial_y u)/f$. We assume $\partial_x v \ll \partial_y u$, so that $-\partial_y u$ approximates ξ . In Figure 6 we plot the ratio of $\partial_y u/f$, approximating $-\xi/f$, as a function of *y* for both the April and June experiments. The scale at which we estimate and resolve $\partial_y u$ is about 3 km. Freshwater discharge rates are different (Table 2), the bulk buoyancy and volume fluxes are in opposite directions, the winds over the shelf are weakly onshore in April and strongly alongshore in June [Münchow and Garvine, 1993]; however, the distribution of lateral shear is nearly the same. The strong shear is thus a robust feature of the flow in the source region. At about 8 km from the Delaware coast the magnitude of the lateral shear is almost as large as the Coriolis parameter *f*; that is, the magnitudes of relative and planetary vorticities are similar, and the Rossby number is 0(1). We thus conclude that nonlinear inertial forces are an important part of the dynamics of the source region. As they appear to be small in the across-channel momentum balance (Table 1), it is likely that they are important only in the along-channel momentum balance.

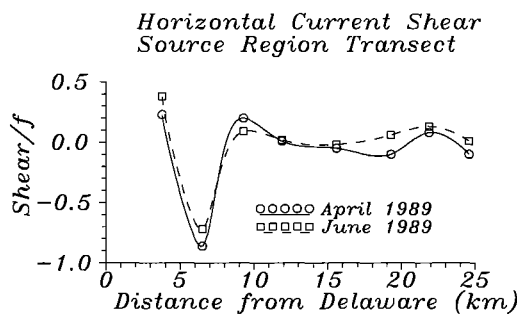


Fig. 6. Horizontal current shear across transect B. We show data from both April and June 1989. The shear is scaled by the planetary vorticity (Coriolis parameter) *f*.

TABLE 2. Scales and Parameters for the Source Region

	March	April	June	Mean
L_D , km	4.4	6.3	7.3	6.2
L_i , km	0.8	1.1	1.0	1.0
L , km	8.0	8.0	8.0	8.0
U , cm/s	7.2	9.9	9.0	8.7
S	0.30	0.64	0.93	0.62
F	0.17	0.17	0.13	0.16
ϵ	0.09	0.14	0.13	0.12
max, ξ/f	0.5	0.9	0.7	0.7
Discharge, m^3/s	150	350	700	400
Wind, m/s	3	1	5	

Many analytical and numerical models of buoyant discharges require specification of the distribution of potential vorticity. Here we just mention two. Modeling channel flows, *Whitehead* [1989] assumes a reservoir of constant potential vorticity. The model correctly predicts the horizontal density differences and the position of a front at the mouth of the Chesapeake Bay. Powerful numerical tools such as contour dynamics [*Stern*, 1989] crucially depend on the assumption of locally homogeneous regions of potential vorticity in barotropic flows. By estimating the potential vorticity distribution, we test whether such models can be applied to the outflow from the Delaware Estuary.

The potential vorticity at a location y is

$$P(y) = [\xi(y) + f] \partial_z \rho(y) / \rho_0. \quad (13)$$

We approximate the vertically averaged relative vorticity ξ as $-\partial_y u$, as above, whereas we estimate the vertically averaged, subtidal vertical density gradient $\partial_z \rho$ from a linear least squares fit to vertical density profiles from CTD casts. In Figure 7 we then present the distribution of potential vorticity across the source region. For each station we averaged the results from the experiments of March, April, and June together. The mean \bar{P} and the standard deviation are shown as the solid curve and the vertical bars respectively in Figure 7. The mean potential vorticity varies considerably across the mouth of the estuary within 10 km from the Delaware coast. The large gradient of properties in the source region shows here as the maximum of potential vorticity magnitude which coincides with the maximum of relative vorticity magnitude. The potential vorticity exhibits this maximum consistently in March, April, and June. We thus conclude that one may not apply uniform potential vorticity models to the outflow from the source region.

3.3. Dynamical Parameters

We first estimate the width L of the subtidal buoyant outflow from the mean density transect data (Figure 3). During each experiment L was 8 km and the internal deformation radius L_D varied between 4 and 7 km from March to June 1989 (Table 2). The Burger number S was then $O(1)$. For an inviscid, steady flow over topography, *Hogg* [1973] showed that moderate stratification ($S \approx 1$) limits the effect that a bumpy bottom exerts on the surface flow through vortex tube stretching. The relative vorticity within the water column from such stretching is then depth-dependent, the flow becomes fully three-dimensional, and the surface flow is little affected by the bottom topography.

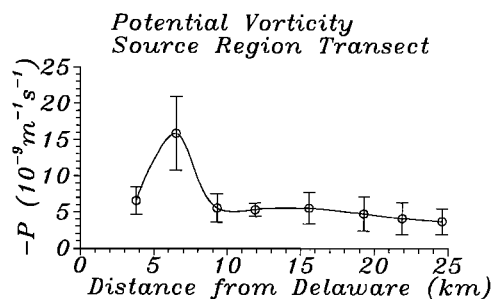


Fig. 7. Potential vorticity across transect B. The open circles represent the mean value from the March, April, and June 1989 experiments. The vertical bars indicate 1 standard deviation from the mean.

The inertial radius $L_i = U/f$, however, is much smaller than L and the Rossby number ϵ calculated from the subtidal velocity scale of the outflow is always smaller than 0.15 (Table 2). Although the smallness of this parameter indicates a weak role for nonlinear inertial forces relative to the Coriolis force, the ratio ξ/f is a better measure of the nonlinearity of the flow, because the lateral velocity gradient rather than the velocity itself is large in the source region. We thus argue that nonlinear inertial forces are important in the source region even though their contribution to the lateral momentum balance (Table 1) is small. The situation is similar to that of the Gulf Stream. To first order, that flow is in geostrophic balance in the across-stream direction. The front at the western edge of the Gulf Stream, however, implies large lateral velocity gradients. Hence, even though the along-stream velocity component is almost in geostrophic balance, the along-stream momentum balance is not [*Garvine*, 1984]. We thus argue that in our source region, as near the Gulf Stream front, both rotation and nonlinear advection are important.

The vertical Ekman number, our final parameter, measures the frictional effects of the flow. The Ekman number depends upon an eddy viscosity that is generally unknown. We thus use a bulk formula to give an order of magnitude estimate of this parameter. For tidally dominated channel flows [*Bowden*, 1967] proposed the formulation $A = C_d U_t D$ for the vertical eddy viscosity A , where C_d , U_t , and D are a drag coefficient, a tidal velocity scale, and a depth scale, respectively. *Ianniello* [1977] argues that the same formulation may be used for subtidal flows also. Hence, we take $U = 0.5 \text{ m/s}$, $D = 25 \text{ m}$, and $C_d = 0.0002$ and obtain an Ekman number that equals 0.8. Friction thus influences the entire water column as the Ekman layer depth is of the same order as the water depth, that is, $E=O(1)$. We thus conclude that frictional forces contribute to the dynamics of the source region.

In summary, we find that three parameters describe the subtidal flow of the source region. The Burger number of $O(1)$ implies a flow that is moderately stratified; the vorticity ratio ξ/f of $O(1)$ implies a flow in which nonlinear inertial forces contribute to the dynamics; and, finally, the Ekman number of $O(1)$ implies a flow that is embedded within a single frictional layer. The Froude number that we compute from the Rossby and Burger numbers, however, is always smaller than 1 (Table 2) and thus implies a subcritical flow. This flow is shore trapped. Its width scales with the internal deformation radius that is small relative to the width of the channel.

4. THE PLUME REGION

4.1. Observations

We studied the plume region downstream of the source region during four separate experiments in 1989. The mean flow is downstream in the direction of Kelvin wave phase propagation, the width of the current increases from one to several internal deformation radii, and in the absence of strong upwelling favorable winds the plume waters generally extend from the surface to the bottom. Fronts are weaker than they are in the source region, but large horizontal velocity and density gradients persist. The frictional diffusion of relative vorticity that has been generated in the source region explains both the widening of the plume and weakening

of lateral property gradients.

In Figure 8 we depict wind, discharge, and 6 m depth current time series for the period from March to June of 1989. For ease of viewing we subjected the data to a Lanczos low-pass filter with a cutoff period near 5 days. This filter removes the high-frequency, dominantly wind-driven motion [Münchow and Garvine, 1993]. We observe a downstream flow that opposes the generally upwelling favorable local winds. The discharge from the Delaware River increases toward the end of the time series, as do the downstream currents.

Salinity is an excellent tracer of estuarine waters on the shelf. In our study area, density varied nearly linearly with salinity. Since buoyant plume waters generally extend to the bottom, surface salinity maps catch most features of the buoyant outflow on the shelf. In Figure 9 we reproduce the horizontal and vertical distribution of salinity near the Delaware Estuary observed by *H. Haskin* (unpublished manuscript, 1953). It took him about three weeks to complete the survey in early March 1952, using one of the earliest operational salinity-temperature-depth (STD) systems. The convoluted and banded structure of the light water along the Delaware and Maryland shores is the first recorded (but unpublished) evidence of the coastal current. From the vertical transects across the shelf, we infer that a large salinity gradient at about 15 km from the coast separates buoyant inner

shelf from ambient shelf waters. Most important for our discussion here, however, is the initial widening of the buoyant plume and the extension of the inshore buoyant waters to the bottom.

For March and May 1989 (Julian days 73 and 115 in Figure 8) we depict in Figure 10 two maps of the surface salinity field that we completed, each within 19 hours. While the local winds during the two experiments were comparable, the freshwater discharge rates prior to the experiments were an order of magnitude different. In March, 150 m³/s of fresh water entered the estuary whereas in May more than 2000 m³/s flooded the estuary and the shelf (Figure 8). Here, however, we stress similarities rather than differences. The plume widens on the shelf, narrows farther downstream, and contacts the bottom in both cases. We have five more maps (not shown) that reveal similar characteristics; strong vertical stratification occurs only if upwelling favorable winds exceed 7 m/s. Buoyant plume waters then move offshore near the surface and denser shelf waters move onshore at depth [Münchow and Garvine, 1993]. This process tilts isopycnals and induces vertical stratification. In the absence of winds, buoyant waters extend to the bottom (Figures 9 and 10).

Mean currents are those at periods larger than the observational period. They are the most effective in transporting material and are always of prime interest. Garvine [1991] analyzed data from current meter moorings deployed on the

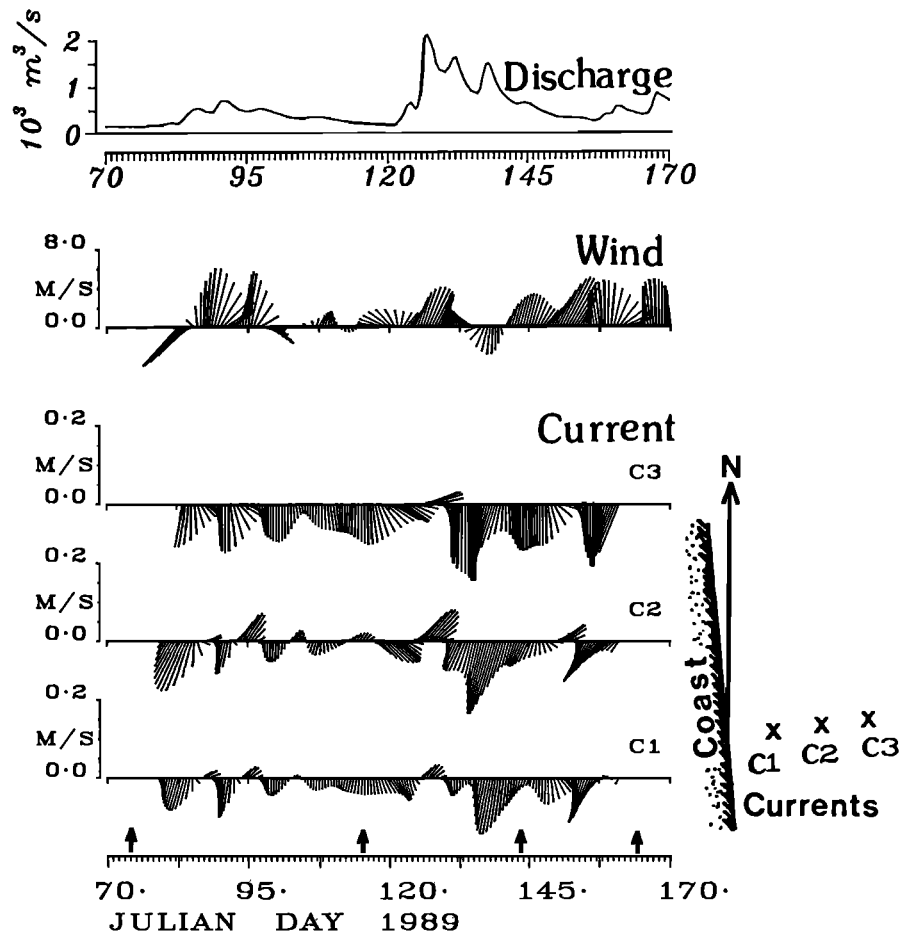


Fig. 8. Discharge, wind, and current time series. Shown are freshwater discharge of the Delaware River, winds at EB9 (see Figure 1), and current vectors off the coast of Delaware 6 m below the surface (see Figure 1 for locations). Arrows on the bottom time axis indicate times of the ship-board surveys.

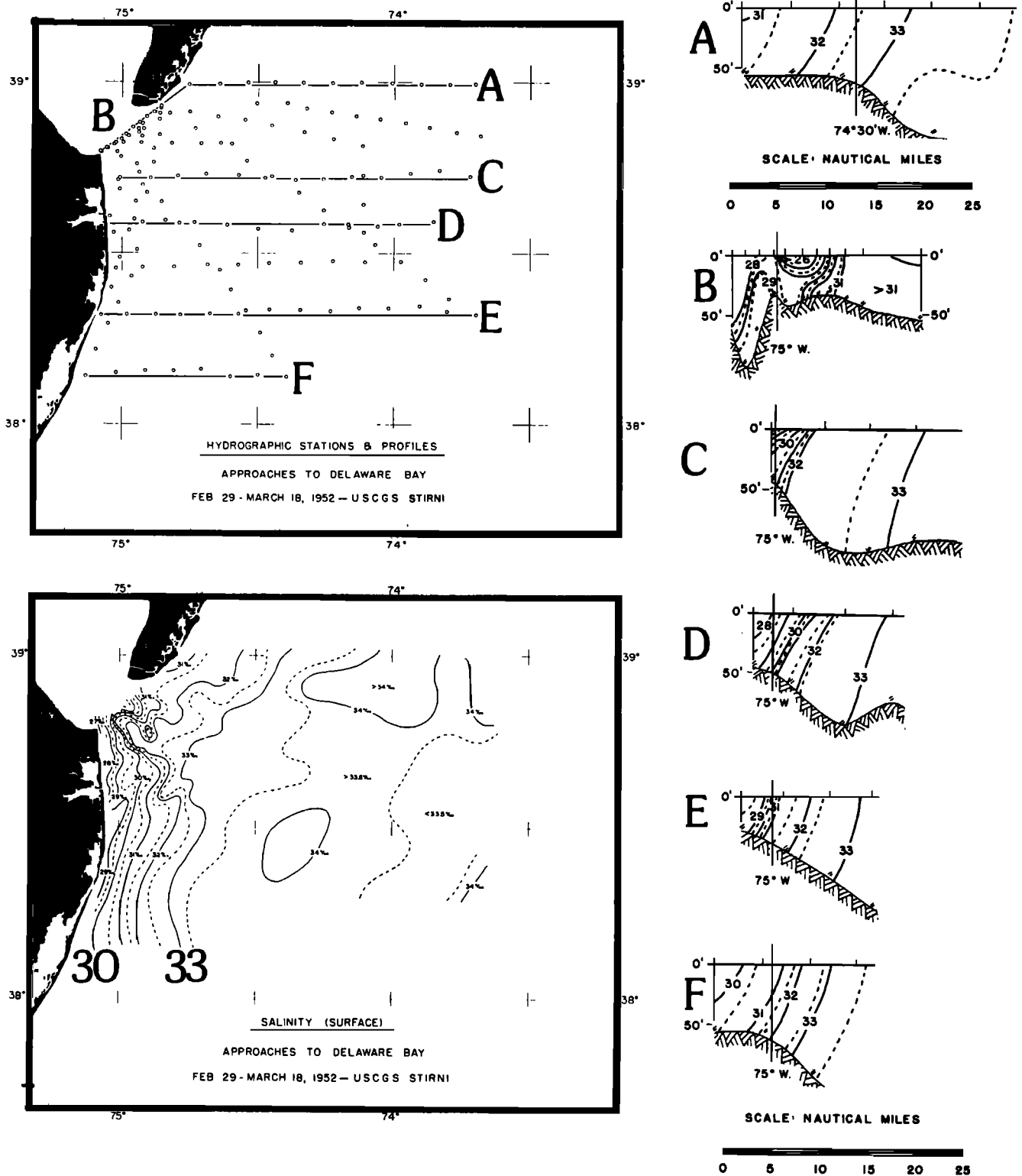


Fig. 9. Salinity distribution in March 1952. Reproduced from H. Haskin (unpublished manuscript, 1953).

shelf 30 km from the mouth of the Delaware Estuary. In Figure 11a we show mean currents from that study along with those from this one. We thus assume a stationary flow at very long time-scales. Upstream of the Delaware Estuary, mean currents are weak and directed either onshore or toward the estuary. Surface currents on the upstream transect A do not have a preferred direction at the 95% confidence

level [Mardia, 1972] and are therefore not shown. Downstream of the estuary they are strong and directed along the shore in the direction of Kelvin wave phase propagation. The latter flow indicates the Delaware Coastal Current. It is strongest offshore where the largest lateral property gradients occur (Figure 10). All error bars reflect 95% confidence limits for speed [Kundu and Allen, 1976] and direction [Mar-

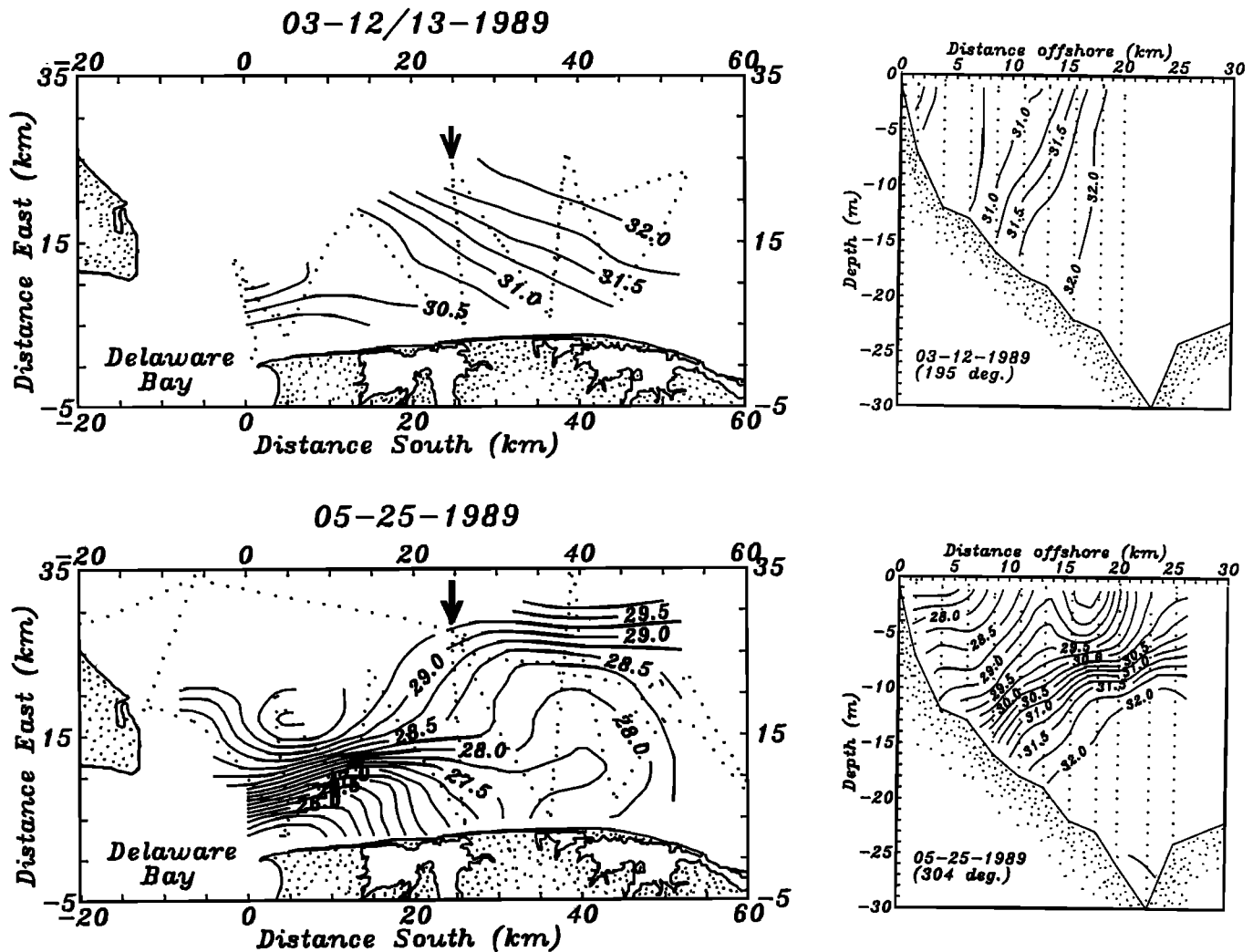


Fig. 10. Two maps of surface salinity for the plume region. Dotted lines indicate the ship track along which the data have been collected. To the right of each map we depict the vertical salinity at a transect whose location we indicate with an arrow. The contour interval is 0.25 psu.

dia, 1972] independently. Off Delaware there is a 3-month mean surface flow with maximum speeds of 8 cm/s. The current is sheared laterally: it reduces to 4 cm/s near the coast.

The spatial structure of the subtidal currents differs from that of the mean. In Figure 11b we show the principal axes of subtidal variability from moored S4 current meters. The axes are strongly polarized along isobaths and are very similar on both sides of the estuary. The currents on the major axis are between 7 and 11 cm/s. Münchow and Garvine [1993] attribute the different spatial structure of the mean and the principal axes to two different forcing processes. At long timescales of several weeks, they argue, buoyancy forcing rivals the wind-driven circulation. Buoyancy forcing, however, varies in space as it depends upon the distance from an upstream buoyancy source. At short timescales of a few days, in contrast, local wind forcing becomes dominant, but local winds do not vary at the spatial scales that we consider here. Finally, interpreting Figure 11b as the current response to winds at short timescales, we find a uniform response to the uniform winds even at the spatial scales considered here. Hence Figures 11a and 11b probably reflect the circulation induced by buoyancy and local wind forcing,

respectively; however, other forcing mechanisms contribute to the current variance also.

4.2. Dynamics

As in section 3, we will next estimate lateral velocity differences that we interpret as measures of the relative vorticity of the flow. In contrast to the source region, where we relied on ADCP data alone, here we estimate horizontal current shears from current meter and drifter data also. During a 40 day period we deployed, retrieved, and redeployed between four and seven drifters on seven occasions. The drifters sampled the velocity field of the coastal current at 2 m depth during both upwelling and down-welling favorable winds [Münchow and Garvine, 1993]. In the mean, however, drifter tracks opposed the local winds as did currents from moored instruments (Figure 8). We estimated the degrees of freedom of the drifter data set from the Lagrangian autocorrelation function and found that velocities are decorrelated after about a day [Münchow and Garvine, 1993]. We next obtained Eulerian current estimates from the drifters by averaging all drifter velocities along the entire plume region (40 km) in across-shelf spatial bins that were

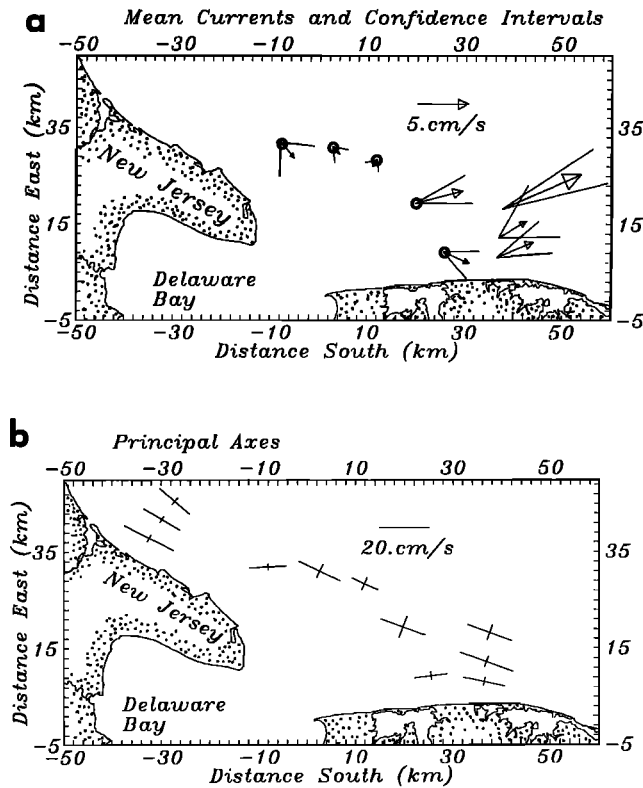


Fig. 11. Subtidal currents from near surface. S4 current meters: (a) record mean current vectors and 95% confidence limits for speed and direction; (b) principal axes for the deviation from the record mean. The two lines besides the arrow represent the upper 95% and lower 95% confidence limit for direction. The lengths of these lines represent the mean speed, that is, that of the arrow, plus the 95% confidence limit for the speed. Data from 1985 to 1987 are indicated by open circles.

3.5 km wide. In Figure 12 we show only those mean currents that have both a preferred direction at the 95% confidence level [Mardia, 1972] and at least eight degrees of freedom. The linear fit of the alongshore velocity with across-shelf distance y explains 99% of the variance and gives a ratio of $\partial_y u / f$ of about -0.14, corresponding to cyclonic relative vorticity, with greatest downshelf velocity at the limit of drifter observations about 10 km from the coast. Farther inshore we find from ADCP data positive current shears that imply anticyclonic relative vorticity, but, as we discuss next, these

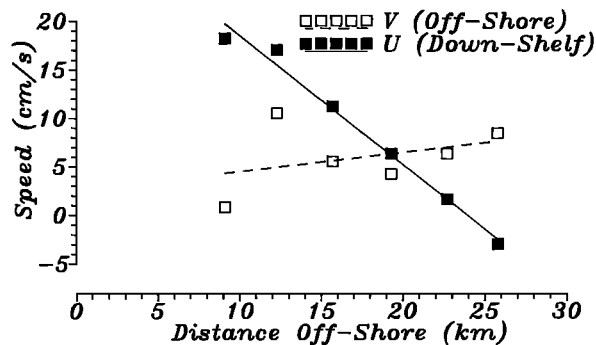


Fig. 12. Across-shore current profile from drifter data. Data averaged in bins 40 km (alongshore) and 3.5 km (across-shore) wide. Note the almost linear decrease of the downshelf velocity component toward offshore.

results are only marginally significant.

In Figure 13 we depict the shear estimates from the drifter data along with those we computed from S4 current meter and ADCP data on transect C. We estimated current shears by differencing velocity estimates from adjacent stations. For the S4 currents we used the mean currents (Figure 11a) to estimate the shear. The error bars reflect the uncertainty due to two current uncertainties at the 95% confidence level. For the ADCP data we depict shear estimates and their uncertainties as the mean and standard deviation from three surveys, respectively. The magnitude of the shear increases from zero 3 km from the coast to about $0.15f$ at 8 km offshore. Farther offshore the shear decreases. The error bars, however, indicate that many of our estimates do not differ significantly from zero. Nevertheless, the small magnitude of the lateral shear of the flow in the plume region contrasts with that for the source region, where it was large. Interpreting this shear as an estimate of relative vorticity we thus conclude that the along-shelf flow in the plume region is consistent with linear dynamics.

4.3. Dynamical Parameters

We summarize the plume region in terms of Burger, Rossby, and Ekman numbers. The differences between the source and plume region emerge from these parameters. In the plume region both the Rossby and the Burger numbers are much smaller than unity (Table 3). Small Rossby numbers indicate that the nonlinear advective terms are small, consistent with the observed small ratio of relative to planetary vorticity (Table 3). Small Rossby numbers are also consistent with the finding that Eulerian and Lagrangian integral timescales are similar [Münchow and Garvine, 1993].

The current widens on the shelf beyond the internal deformation radius such that the Burger number S becomes small relative to unity, that is, $S \rightarrow \epsilon$. The dynamical implications of this observation are important. For a steady, inviscid flow over topography, Hogg [1973] found that vortex tube stretching generates relative vorticity that is independent of depth if vertical stratification is weak: that is, $S \rightarrow \epsilon \ll 1$. Bottom topography thus should affect the entire flow here. Hogg [1973] further showed that the weak vertical stratification that does exist suffices to support the vertical current shear through thermal wind balance. The geostrophy of the alongshore flow, however, does not necessarily imply that quasi-geostrophic dynamics holds. Cushman-Roisin [1986]

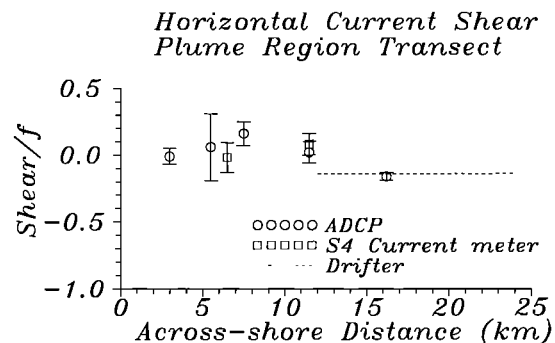


Fig. 13. Horizontal current shear $\partial_y u$ across the plume region scaled by the Coriolis parameter f . We depict data from ADCP stations (circles), current meters (boxes), and drifters (dashed line). Note that the shear is always small relative to f . The plume width L is generally larger than 20 km (see Table 3).

TABLE 3. Scales and Parameters for the Plume Region

	March	April	June	Mean
L_D , km	1.8	6.3	10.0	6.0
L_i , km	1.0	0.8	0.5	0.7
L , km	10	25	25	20
U , cm/s	9.0	7.2	4.5	6.9
S	0.03	0.06	0.06	0.05
F	0.57	0.12	0.05	0.25
ϵ	0.10	0.03	0.05	0.06
max, ξ/f	0.3	0.1	0.2	0.2
Discharge, m ³ /s	150	350	700	400
Wind, m/s	3	1	5	

argued for a frontal geostrophic model if $S \rightarrow \epsilon$ that allows finite upper-layer perturbations. In section 5 we will discuss this point further.

As in the source region, the dependence of the Ekman number on a poorly known eddy viscosity bars us from estimating this parameter with much confidence. Münchow [1992], however, fitted Ekman layer solutions to vertical ADCP current profiles and found the best agreement between theory and observations for vertical Ekman numbers between 0.4 and 0.8. As in the source region the coastal current is thus imbedded within a frictional layer that occupies the entire water column.

In summary, we describe the plume region with three independent parameters. Both the Burger and the Rossby number are small relative to unity while the Ekman number is $O(1)$. This implies a weakly stratified flow in which nonlinear inertial forces do not contribute to the dynamics while frictional ones do. The Froude number that we computed from the Burger and Rossby number (Table 3), indicates a subcritical flow. The coastal current, moreover, is still trapped near the shore even though its width is about three internal deformation radii.

5. DISCUSSION

The influx of buoyant waters from the Delaware Estuary into the coastal ocean affects the dynamics there profoundly. We found two dynamically different regimes, namely a source and a plume region. Münchow [1992] suggested a third region farther downstream yet, where, instead of a wide and diffuse plume region, a narrow but unstable coastal jet finally forms. This part of the Delaware Coastal Current is the subject of an ongoing field study.

The major results of this study are summarized in Figure 14. It depicts the alongshore variability of the Burger number, the Rossby number, and the ratio between the lateral shear and the planetary vorticity f . We interpret the shear as an estimate of the relative vorticity. Near the source of the coastal current, both the vorticity ratio and the Burger number are $O(1)$. The former implies that the flow is nonlinear, whereas the latter indicates that the width of the current scales well with the deformation radius and that vertical stratification limits the impact of vortex tube stretching by bottom topography. In both the source and the plume region the flow appears to be geostrophic in the across-stream direction even though our tests of geostrophy were inconclusive. Nonlinear advection through $\partial_y u$, however, is important in the source region where the buoyant

waters from the estuary turn anticyclonically. The subtidal outflow separates from one coast and we find seaward flowing, positively buoyant estuarine water alongside landward flowing ambient shelf water.

In the plume region both these parameters decrease and become much smaller than unity. This implies that the flow becomes linear and that either frictional or instability processes or both widen the coastal current beyond the deformation radius. Consistent with this, both ϵ and the ratio $\partial_y u/f$ (labeled shear/ f in Figure 14a) are much smaller than unity. Burger number S and relative vorticity ξ , however, become smaller also, that is,

$$\epsilon \leq S \simeq |\partial_y u| / f \simeq |\xi| / f \ll 1.$$

In a series of papers Cushman-Roisin argues that frontal geostrophic regimes exist when $\epsilon < S \ll 1$ [Cushman-Roisin, 1986; Chassignet and Cushman-Roisin, 1991; Cushman-Roisin et al., 1992]. Such geostrophic dynamics allows finite layer perturbations and the surfacing of isopycnals. The vorticity equation then, these authors argue, is not quasi-geostrophic because the vortex tube stretching mechanism dominates over the diffusion of relative vorticity. Applying these arguments to our case implies that although the primary across-shelf momentum balance is geostrophic, the vorticity equation is not quasi-geostrophic. However, since the dynamical parameter S decreases by a factor of almost 10 from the source to the plume region (Figure 14a), we interpret the latter as one of dynamic transition. Frictional torques begin to contribute to the vorticity balance as they cause widening of the buoyant waters through the diffusion of relative vorticity. Potential vorticity is thus not a conserved property of the flow. The current turns anticyclonically and transforms from a nonlinear, moderately

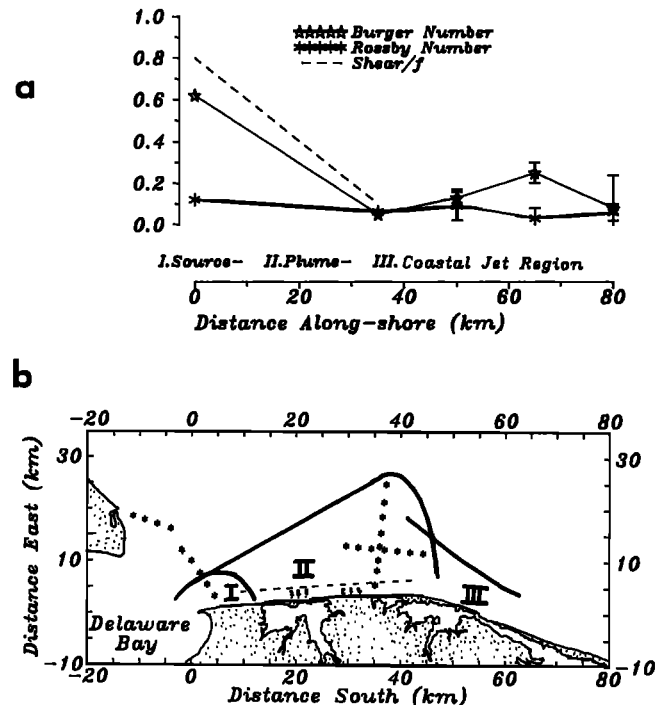


Fig. 14. Parameters and sketch of dynamical regions. (a) Parameters of the Delaware Coastal Current versus along-shelf distance; (b) conceptual sketch of the different regions. The stars in (b) represent major CTD and ADCP stations. The parameter values for the third, the "coastal jet" region, are from Münchow [1992].

stratified jet to a linear, weakly stratified current. In the plume region the structure of the Delaware Coastal Current includes an offshore zone of enhanced density gradients. Farther downstream yet, all parameters reach almost constant values [Münchow, 1992]. We interpret this as the region where a coastal jet has finally formed. From Figure 14a we thus infer three different regions, which are sketched in Figure 14b.

Many theoretical models of buoyancy driven coastal currents have been proposed over the last decade. They fall into two distinct categories, namely, process studies and general circulation models. The former generally concentrate on some isolated physical aspects of the flow, whereas the latter attempt to resolve many such processes. We first compare the observational results with reduced gravity and frictional models as examples of process studies. Thereafter we compare results from the general circulation models of Galperin and Mellor [1990a, b, c] and Chao [1988a, b] with observations.

Reduced gravity models of coastal ocean circulation generally assume a shallow, buoyant surface layer that is dynamically active above a deep layer where the motion is independently set [Cherniawsky and LeBlond, 1986; Garvine, 1987; O'Donnell, 1990]. One cannot apply these models to the circulation on the shelf off Delaware and Maryland, because here a single buoyant layer occupies the entire water column most of the time. A different but equally inapplicable model is that of Zhang *et al.* [1987]. This quasi-geostrophic model includes thin surface and bottom Ekman layers. The Delaware Coastal Current, however, cannot be quasi-geostrophic, because the "layer perturbations" extend over the entire depth. Quasi-geostrophic theory cannot accommodate such large "perturbations" [Flierl, 1984]. Also, the shallow water depths on the inner shelf do not allow an interior flow which is distinct from surface and bottom boundary layers.

Frictional and steady state models, such as proposed by Heaps [1972] and Vennell and Malanotte-Rizzoli [1990], allow $O(1)$ vertical Ekman numbers, assume a vertically uniform mass field, and contain horizontal density gradients but ignore alongshelf variability, but resolve the resulting vertical current structure. In contrast, Vennell and Malanotte-Rizzoli [1990] solve for the density field as well, model horizontal variability with a stream function, but depth-average all variables. The two models thus address different aspects of density-driven shelf dynamics with friction. Both studies predict velocities almost an order of magnitude smaller than those we observe. They thus appear to model larger-scale aspects of the shelf circulation, that is, large relative to the internal deformation radius L_D . Neither of the frictional models contain as a scale L_D , as they both neglect vertical density variations. In the Delaware Coastal Current we observe small but finite vertical density gradients. These are dynamically important, since they determine L_D , which is the dominant scale of motion.

Chapman and Lentz [1993] designed a series of numerical experiments, all of which allowed the across-shelf advection of buoyancy of a semigeostrophic coastal current. The offshore advection of buoyancy within the bottom Ekman layer maintains the density front through instantaneous overturning. Their model and the proposed physical mechanism is most relevant for the Delaware Coastal Current.

Finally, we compare our observations with results from

two general circulation models. Galperin and Mellor [1990a, b, c] attempted to simulate the dynamics of the Delaware Estuary and the adjacent continental shelf in 1984 as a coupled system as realistically as possible. They employ observed bottom topography and specify tidal, wind, freshwater discharge, and surface heat flux forcing functions. Even though freshwater discharge rates and winds in 1984 and 1989 are comparable, the model results disagree qualitatively with our observations from 1989. We observed a buoyant plume off Delaware under seven different freshwater discharges and mostly upwelling favorable wind conditions. We always found buoyant plume waters downstream, independent of wind direction. In the model simulations of Galperin and Mellor [1990a, b, c] this plume is highly susceptible to local winds, often absent, and occasionally even found upstream. During upwelling-favorable winds the model predicts an upstream-moving buoyant plume on the shelf. During downwelling-favorable winds a few days later no plume waters were found on the shelf. Such model results clash with our observational evidence. We speculate that the specific model application fails because it constrains estuary/shelf interactions by imposing a grid matching algorithm at the mouth of the Delaware Estuary where both the temporal and spatial variabilities are the largest. The model also appears to be too sensitive to wind forcing whereas it is not sensitive enough to buoyancy forcing.

A second, less specific, but carefully designed general circulation model [Chao, 1988b] purposely avoids simulating all aspects of estuary-shelf interaction. It succeeds, however, in realistically reproducing many aspects of the buoyancy driven coastal current that we observe. Chao [1988b] specified the discharge of freshwater at the head of a rectangular estuary which, after reaching the continental shelf, forms a plumelike bulge and a narrow coastal current downstream. These are qualitative features that we observed in the Delaware Coastal Current. The model, however, does not simulate correctly the observed location of the bulge or the vertical structure of observed variables for the Delaware Coastal Current. This outcome may arise from frictional coefficients that are too small for the Delaware Coastal Current, as Chao did not intend that application.

Chao also proposed the use of two nondimensional parameters for a classification of buoyant plumes and coastal currents. The first parameter, a densimetric Froude number, measures nonlinearity and stratification. The second parameter measures the influence of friction. He organized model results with these two parameters and distinguished four different regimes. The flow is either supercritical ($F > 1$) or subcritical ($F < 1$) and either diffusive or nondiffusive. Within this scheme we speculate that the Delaware Coastal Current is diffusive-subcritical. The importance of friction and the relevance of Ekman dynamics, however, remain to be studied.

Acknowledgments. The competent and good-humored crew of the R/V *Cape Henlopen* under their captain Donald McCann enabled us to collect the data set in a most enjoyable fashion. The technical assistance at sea of Timothy Pfeiffer was crucial to analysis of the shipboard data near real time. At sea many friends shared hands and minds, while on land stimulating discussions with David Chapman, John McCalpin, James O'Donnell, and Kuo-Chuin Wong shaped our theoretical arguments. The National Science Foundation funded this study through grant OCE-8816009.

REFERENCES

- Åhlén, K., T. C. Royer, and T. H. George, Multiple dipole eddies in the Alaskan Coastal Current detected with Landsat Thematic Mapper data, *J. Geophys. Res.*, *92*, 13,041-13,047, 1987.
- Beardsley, R. C., and J. Hart, A simple theoretical model for the flow of an estuary onto a continental shelf, *J. Geophys. Res.*, *83*, 873-883, 1978.
- Blanton, J. O., Ocean currents along a nearshore frontal zone on the continental shelf of the eastern United States, *J. Phys. Oceanogr.*, *11*, 1627-1637, 1981.
- Bowden, K. F., Stability effects on turbulent mixing in tidal currents, *Phys. Fluids Suppl.*, *110*, 278-280, 1967.
- Bowman, M. L. and R. L. Iverson, Estuarine and Plume fronts, Oceanic fronts in coastal processes, edited by M. L. Bowman and W. E. Esaias, pp. 87-104, Springer-Verlag, New York, 1978.
- Chao, S.-Y., Wind driven motion of estuarine plumes. *J. Phys. Oceanogr.*, *18*, 1144-1166, 1988a.
- Chao, S.-Y., River forced estuarine plumes. *J. Phys. Oceanogr.*, *18*, 72-88, 1988b.
- Chapman, D. C. and S. Lentz, Trapping of a coastal density front by a bottom boundary layer, *J. Phys. Oceanogr.*, *23*, in press, 1993.
- Chassignet, E. P. and B. Cushman-Roisin, On the influence of a lower layer on the propagation of nonlinear oceanic eddies, *J. Phys. Oceanogr.*, *21*, 939-957, 1991.
- Cherniawsky, J. and P. H. LeBlond, Rotating flows along indented coastlines, *J. Fluid Mech.*, *169*, 379-407, 1986.
- Csanady, G. T., The arrested topographic wave, *J. Phys. Oceanogr.*, *8*, 47-62, 1978.
- Cushman-Roisin, Frontal geostrophic dynamics, *J. Phys. Oceanogr.*, *16*, 132-143, 1986.
- Cushman-Roisin, B., G. G. Sutyrin, and B. Tang, Two-layer geostrophic dynamics, I, Governing equations, *J. Phys. Oceanogr.*, *22*, 117-127, 1992.
- d'Hieres, C. G., H. Didelle, and D. Obaton, A laboratory study of surface boundary currents: Application to the Algerian Current, *J. Geophys. Res.*, *96*, 12,539-12,548, 1991.
- Doyle, B. E. and R. E. Wilson, Lateral dynamic balance in the Sandy Hook to Rockaway Point transect. *Estuarine Coastal Shelf Sci.*, *6*, 165-174, 1978.
- Flierl, G. R., Rossby wave radiation from a strongly nonlinear warm eddy, *J. Phys. Oceanogr.*, *14*, 47-58, 1984.
- Galperin, B. and G. L. Mellor, A time dependent, three-dimensional model of the Delaware Bay and River system, I, Description of the model and tidal analysis. *Estuarine Coastal Shelf Sci.*, *31*, 231-253, 1990a.
- Galperin, B. and G. L. Mellor, A time dependent, three-dimensional model of the Delaware Bay and River system, II, Three-dimensional flow field and residual circulation, *Estuarine Coastal Shelf Sci.*, *31*, 255-281, 1990b.
- Galperin, B. and G. L. Mellor, Salinity intrusion and residual circulation in Delaware Bay during the drought of 1984, Residual Currents and Longterm Transport, edited by R. T. Cheng, pp.467-480, Springer-Verlag, New York, 1990c.
- Garrett, C. and B. Petrie, Dynamical aspects of the flow through the Strait of Belle Isle, *J. Phys. Oceanogr.*, *11*, 376-393, 1981.
- Garvine, R. W., Propagating long waves on oceanic density fronts: An analytic model, *J. Phys. Oceanogr.*, *14*, 1590-1599, 1984.
- Garvine, R. W., Estuary plumes and fronts in shelf waters: A layer model, *J. Phys. Oceanogr.*, *17*, 1877-1896, 1987.
- Garvine, R. W., Subtidal frequency estuary-shelf interaction: Observations near Delaware Bay, *J. Geophys. Res.*, *96*, 7049-7064, 1981.
- Gill, A. E., Adjustment under gravity in a rotating channel, *J. Fluid Mech.*, *77*, 603-621, 1976.
- Griffiths, R. W. and P. F. Linden, The stability of buoyancy driven coastal currents, *Dyn. Atmos. Oceans*, *5*, 281-306, 1981.
- Hansen, D. V. and M. Rattray, Jr., Gravitational circulation in estuaries, *J. Mar. Res.*, *23*, 104-122, 1965.
- Heaps, N. S., Estimation of density currents in the Liverpool Bay area of the Irish Sea, *Geophys. J. Roy. Astron. Soc.*, *30*, 415-432, 1972.
- Hickey, B. M., R. E. Thompson, H. Yih, and P. H. LeBlond, Wind and buoyancy driven fluctuations in the Vancouver Island Coastal Current, *J. Geophys. Res.*, *96*, 10,507-10,538, 1991.
- Hogg, N. G., On the stratified Taylor column, *J. Fluid Mech.*, *58*, 517-537, 1973.
- Ianniello, J. P., Tidally induced residual currents in estuaries of constant breadth and depth, *J. Mar. Res.*, *35*, 755-786, 1977.
- Johannessen, J. A., E. Svendsen, S. Sandven, O. M. Johannessen, and K. Lygre, Three dimensional structure of meso scale eddies in the Norwegian Coastal Current, *J. Phys. Oceanogr.*, *19*, 3-19, 1989.
- Johnson, W. R., T. C. Royer, and J. L. Luick, On the seasonal variability of the Alaskan Coastal Current, *J. Geophys. Res.*, *93*, 12,423-12,437, 1988.
- Kundu, P. K. and J. S. Allen, Some three dimensional characteristics of low frequency current fluctuations near the Oregon coast, *J. Phys. Oceanogr.*, *6*, 181-199, 1976.
- Mardia, K. V., *Statistics of Directional Data*, Academic, San Diego, Calif., 1972.
- Masse, A. K. and C. R. Murthy, Observations of the Niagara River thermal plume (Lake Ontario, North America), *J. Geophys. Res.*, *95*, 16,097-16,110, 1990.
- Mertz, G., M. J. El-Sabh, D. Proulx, and A. R. Condal, Instability of a buoyancy driven coastal jet: The Gaspé Current and its St. Lawrence precursor, *J. Geophys. Res.*, *93*, 6885-6893, 1988.
- Mork, M., Circulation phenomena and frontal dynamics of the Norwegian Coastal Current, *Philos. Trans. R. Soc. London Ser. A302*, 635-647, 1981.
- Münchow, A., Formation of a buoyancy driven coastal current, Ph.D. Dissertation, Univ. of Delaware, Newark, 1992.
- Münchow, A., A. K. Masse, and R. W. Garvine, Astronomical and nonlinear tidal currents in a coupled estuary shelf system, *Cont. Shelf Res.*, *12*, 471-498, 1992a.
- Münchow, A., R. W. Garvine, and T. F. Pfeiffer, Subtidal currents from a shipboard acoustic doppler current profiler in tidally dominated waters, *Cont. Shelf Res.*, *12*, 499-515, 1992b.
- Münchow, A. and R. W. Garvine, Buoyancy and wind forcing of a coastal current, *J. Mar. Res.*, *51*, 293-322, 1993.
- Nihoul, J. C. J. and F. C. Rooday, The influence of tidal stress on the residual circulation, *Tellus*, *27*, 484-489, 1975.
- O'Donnell, J., A numerical technique to incorporate frontal boundaries in two dimensional layer models of ocean dynamics, *J. Phys. Oceanogr.*, *18*, 1584-1600, 1988.
- O'Donnell, J., The formation and fate of a river plume: A numerical model, *J. Phys. Oceanogr.*, *20*, 551-569, 1990.
- Pedlosky, J., *Geophysical Fluid Dynamics*, 2nd ed., Springer-Verlag, New York, 1987.
- Royer, T. C., Observations of the Alaskan Coastal Current, Coastal Oceanography, edited by H. Gade, A. Edwards, and H. Svendsen, pp.9-30, Plenum, New York, 1983.
- Simpson, J. H. and A. E. Hill, The Scottish Coastal Current, in The Role of Freshwater Outflow in Coastal Marine Ecosystems, edited by S. Skreslet, *NATO ASI Ser., G*, *7*, pp.295-308, 1986.
- Simpson, J. H., W. G. Bos, F. Schirmer, A. J. Souza, T. P. Rippeh, S. A. Jones and D. Hydes, Periodic stratification in the Rhine ROFI in the North Sea, *Oceanol. Acta.*, *16*, 23-32, 1993.
- Simpson, J. H., E. G. Mitchelson-Jacob, and A. E. Hill, Flow structure in a channel from an Acoustic Doppler Current Profiler, *Cont. Shelf Sci.*, *10*, 589-603, 1989.
- Stern, M. E., Evolution of locally unstable shear flow near a wall or coast, *J. Fluid Mech.*, *198*, 70-99, 1989.
- Tang, C. L., Mixing and circulation in the north western Gulf of St. Lawrence: A study of a buoyancy driven current system, *J. Geophys. Res.*, *85*, 2787-2796, 1980.
- van der Giessen, A., W. P. M. de Ruijter, and J. C. Borst, Three dimensional current structure in the Dutch coastal zone, *Neth. J. Sea Res.*, *25*, 45-55, 1990.
- Vennell, M. R. and P. Malanotte-Rizzoli, The influence of a steady baroclinic deep ocean on the shelf: The vertical well-mixed case, *J. Phys. Oceanogr.*, *20*, 489-505, 1990.
- Weaver, A. J. and W. Hsieh, The influence of buoyancy flux from estuaries on the continental shelf circulation, *J. Phys. Oceanogr.*, *17*, 2127-2140, 1987.
- Whitehead, J. A., Internal hydraulic control in rotating fluids—Applications to the oceans, *Geophys. Astrophys. Fluid Dyn.*, *48*, 169-192, 1989.
- Whitehead, J. A. and D. C. Chapman, Laboratory observations

- of a gravity current on a sloping bottom: The generation of shelf waves, *J. Fluid Mech.*, 172, 373-399, 1986.
- Woods, A. W., and R.C. Beardsley, On the barotropic discharge of a homogeneous fluid onto a continental shelf, *Cont. Shelf Res.*, 8, 307-327, 1988.
- Zhang, Q. H., G. S. Janowitz, and L. J. Pietrafesa, The interaction of estuarine and shelf waters: A model and applications, *J. Phys. Oceanogr.*, 17, 455-469, 1987.

R. W. Garvine, University of Delaware, College of Marine Studies, Newark, DE 19716-3501.

A. Münchow, Center for Coastal Studies, Scripps Institution of Oceanography, La Jolla, CA 92093.

(Received June 23, 1992;
revised May 12, 1993;
accepted June 22, 1993.)